Design and Development of a Miniaturized Multiband Patch Antenna Incorporating Metamaterials for IoT Applications

Tatenda Thomas Chigwende
Department of Electrical Engineering, Pan African University Institute for Basic Sciences, Technology and Innovation, hosted at Jomo Kenyatta University of Agriculture and Technology, Nairobi, Kenya
thomas.tatenda@students.jkuat.ac.ke (corresponding author)

Dominic Konditi
School of Electrical and Electronic Engineering, Faculty of Engineering and Built Environment, Technical University of Kenya (TU-K), Nairobi, Kenya
konditidbo@gmail.com

Aliyu Danjuma Usman
Department of Telecommunication Engineering, Faculty of Engineering, Ahmadu Bello University, Zaria, Nigeria
adusman@abu.edu.ng

Received: 5 January 2026 | Accepted: 13 February 2026

 DOI: https://doi.org/10.48084/etasr.17361

ABSTRACT

This paper presents the design, simulation, and fabrication of a novel compact metamaterial-based patch antenna for Internet of Things (IoT) applications. The antenna operates over four frequency bands: 868 MHz, 2.45 GHz, 4.2 GHz, and 5.8 GHz. The reduction in the size of the antenna was achieved using a parasitic patch along with a combination of Complementary Split Ring Resonators (CSRRs). The total area of the final patch antenna was 40 mm × 46 mm. In addition to achieving miniaturization, the Defected Ground Structure (DGS) and the uniplanar Electromagnetic Band Gap (EBG) array were integrated into the patch antenna to enhance performance by suppressing the surface waves and improving the impedance matching. Simulated and measured results show that the impedance matching is very good at the operating frequencies of 868 MHz, 2.45 GHz, 4.2 GHz, and 5.8 GHz with approximate bandwidths of 7 MHz, 73 MHz, 120 MHz, and 90 MHz, respectively. The antenna was fabricated on a Rogers RO4003C substrate (thickness 1.524 mm, εr = 3.38, tanδ = 0.0027) and the Rohde & Schwarz ZVA50 Vector Network Analyzer (VNA) was used to obtain the measured results and compare them with the simulated results. Good agreement was obtained between the simulated and measured results, confirming the feasibility of the proposed antenna as a suitable candidate for compact, low-power, multiband IoT applications.

Keywords-IoT; multiband antenna; Complementary Split Ring Resonator (CSRR); Defected Ground Structure (DGS); Electromagnetic Band Gap (EBG)

I. INTRODUCTION

A new paradigm is required in light of the explosion of the Internet of Things (IoT), to design "all-in-one" wireless hardware that can support multiple communication standards [1]. New IoT nodes must bridge the gap between long-range Low-Power Wide Area Network (LPWAN) protocols (at 868 MHz) and high data rate standards such as Bluetooth (2.45 GHz) and Wi-Fi (5.8 GHz). As a result, a significant barrier exists due to the inherent trade-off between antenna size and radiation efficiency.

At sub-GHz frequencies, conventional patch antennas are typically too large to fit in a compact device. Conversely, miniaturizing patch antennas often leads to very narrow bandwidth and/or very poor gain [2, 3].

Recently, many researchers have investigated various ways to create multiband functionality in small sizes. Some examples include fractal geometries which provide a longer electrical current path; for example, a third iteration Koch design demonstrated resonant frequencies of 868 MHz, 2.4 GHz, and 6 GHz [4]. However, designs employing fractals may exhibit reduced performance stability at higher frequency bands (e.g.,

5.8 GHz), and typically lack built-in methods to mitigate surface wave interference. Other metamaterial-inspired structures, such as Complementary Split Ring Resonators (CSRRs) and Defected Ground Structures (DGSs), have emerged as superior alternatives for sub-wavelength resonance and size reduction [5, 6]. For example, recent studies utilizing Rectangular CSRRs (RCSRRs) achieved size reductions of over 46% when compared to traditional patch antennas; however, they were limited to the GHz bands (i.e., 2.4 GHz and 5.8 GHz) and did not address the 868 MHz band essential for long-range IoT connectivity [5, 7, 8].

Although great progress has been made recently, there is currently a gap in the literature concerning the simultaneous integration of sub-GHz (868 MHz) support with high-frequency GHz bands in a single-layer planar design without losing gain or significantly increasing footprint area. Although some wearable LoRa antennas have effectively supported the 868 MHz band with high efficiency, they are primarily single-band antennas and thus unsuitable for use in multi-standard gateways [9]. On the other hand, high-frequency Multiple-Input Multiple-Output (MIMO) and 5G-IoT antennas achieve excellent isolation and gain at 28 GHz or 5.8 GHz, yet entirely ignore the sub-GHz requirements of the LPWAN ecosystem [8, 10, 11]. Furthermore, the challenge of maintaining a consistent radiation pattern and gain across such widely-spaced frequencies (868 MHz to 5.8 GHz) remains largely unresolved.

More recent studies have extended these limits even further. A wearable Coplanar Vivaldi Antenna (CVA) with an overall size of 60 mm × 60 mm was designed for the detection of toddler stunting [12]. The authors were able to achieve a simulated bandwidth of 133.17% (1.98–3.76 GHz and 5.27–10.84 GHz) and a peak gain of 7.858 dBi through optimization of the cavity radius and corrugations. Although this represents a significant advance in antenna size, the design is specifically intended for Ultra-Wideband (UWB) sensing and does not provide discrete sub-GHz support. Second, the size of the antenna is 49% larger than the design proposed in this study, which also includes the 868 MHz band as part of its hybrid CSRR-patch design.

Additionally, other authors proposed a textile-based CVA for medical IoT application that measures 50 mm × 50 mm, operates between 2.6 GHz and 8.7 GHz, and provides a 107.5% bandwidth and 6.35 dBi gain [13]. Although flexible, it completely lacks support of the sub-GHz band. In the extreme miniaturization trend, other authors introduced a super-compact UWB monopole antenna (15 mm × 17 mm) covering 3.026–12.556 GHz with a high radiation efficiency of about 90% [14]. However, the design does not cover resonance at the 868 MHz or 2.45 GHz bands because of its exclusive focus on UWB sensing.

For 5G sub-6 GHz applications, other authors used the Theory of Characteristic Modes (TCM) for a flexible metasurface MIMO antenna with a volume of 70 × 25 × 0.4 mm³, achieving greater than 3 dBi gain over a 2,700 MHz bandwidth. However, the design lacks compatibility with legacy sub-GHz IoT systems [15]. Interference mitigation was the subject of other authors, who used a quintuple band-notched UWB antenna with dimensions of 38 × 38 × 0.8 mm³ that employed dual Elliptical Split-Ring Resonators (ESRRs) etched into the monopole radiator and Electromagnetic Band Gap (EBG) structures to reject Wireless Local Area Networks (WLANs) and C-band signals across 3.1–10.6 GHz [16]. A major gap in [16] is its "subtractive" nature; it filters existing bands rather than creates them. In contrast, our work uses metamaterials for "additive" resonance creation, thereby generating discrete peaks at 868 MHz and 2.45 GHz while employing EBG arrays for surface wave suppression. Finally, while other authors employed machine learning to estimate parameters for metamaterial antennas, the physical implementation of a quad-band "all-in-one" gateway antenna is still primarily unaddressed [17].

The principal objective of this project is to develop a highly miniaturized triple-band (868 MHz, 2.45 GHz, and 5.8 GHz) patch antenna by integrating three different metamaterial-inspired structures: CSRRs for extreme sub-GHz miniaturization, a DGS for impedance matching, and a uniplanar EBG array for surface-wave suppression. This study demonstrates that a hybrid approach will yield a compact footprint of 40 mm × 46 mm and an additional emergent fourth resonance at 4.2 GHz that can be used for private 5G applications. Experimental verification shows that the designed antenna presents a versatile, multi-protocol solution for the next generation of heterogeneous IoT environments.

II. MATERIALS AND METHODS

A. Mathematical Model and Design Specifications

To determine the preliminary size of the radiating element of the proposed antenna, a transmission line model was used [18]. Therefore, the width (Wp) and length (Lp) of a rectangular microstrip antenna can be determined by empirical equations that consider the working frequency (fr), substrate height (h), and the relative permittivity (εr) of the substrate. In this work, the initial patch was designed to operate at 2.45 GHz, on a Rogers RO4003C substrate (εr = 3.38, tanδ = 0.0027, h = 1.524 mm); the first step was to define an antenna structure on a ground plane (size: 60 mm × 60 mm). The results obtained from these preliminary calculations were taken into account in the successive iterative optimizations to achieve multi-frequency operation and miniaturization of the antenna.

B. Antenna Design Strategy

The design was developed using a three-step iterative multiband design approach, with CST Studio Suite employed to model and simulate each step. With each iteration, the size of the radiating elements was varied to include additional frequency bands while decreasing the footprint as much as possible.

1) Step 1: Multiband Excitation and Parasitic Loading

The 2.45 GHz rectangular patch was used as the starting point on a 60 mm × 60 mm substrate, as shown in Figure 1. This phase established the base design for triple-band performance. Slots were added to the radiator, and a parametric sweep was performed to optimize these slots so that the antenna could operate at two of the three desired frequencies (2.45 GHz and 5.8 GHz). An electromagnetic coupling parasitic patch was then added to excite a low-frequency

resonance at 868 MHz, enabling sub-GHz operation for IoT applications. Parametric sweeps were conducted to find the optimal dimensions and configuration of the parasitic patch such that it functions properly without exceeding the 60 mm × 60 mm footprint.

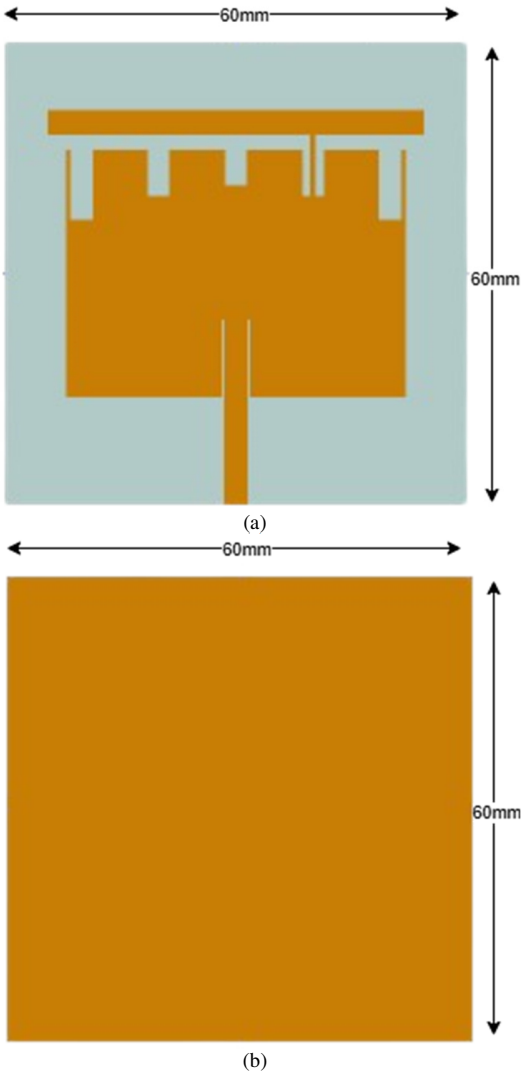

Fig. 1. Structure of the first-stage antenna: (a) top view, (b) bottom view.

2) Step 2: Miniaturization via Complementary Split Ring Resonators

After the triple-band resonance was created, Stage 2 focused on extreme miniaturization to meet the very compact hardware requirements of IoT devices, as shown in Figure 2. Two CSRRs were etched into the main radiating patch of the antenna. The CSRRs provided inductive and capacitive loading at the same time, allowing the resonant frequencies of the antenna to remain the same while reducing the overall footprint by an additional 33% down to 40 mm × 46 mm. This represents a very high level of miniaturization, especially for the 868 MHz frequency band.

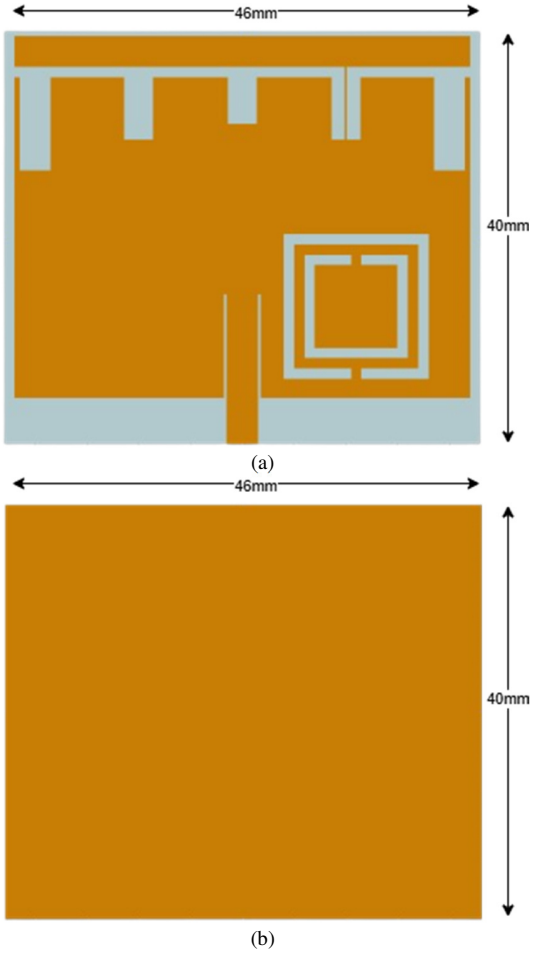

Fig. 2. Structure of second-stage antenna: (a) top view, (b) bottom view.

3) Step 3: Performance Enhancement and Final Optimization

The addition of a DGS and a 1 × 5 uniplanar EBG periodic array improved both impedance matching and radiation efficiency of the final-stage antenna. The DGS influenced the distribution of current on the ground plane, thereby improving the bandwidth. The periodic EBG structure suppressed the generation of surface waves. The final integration of these two structures resulted in an additional fourth resonance at 4.2 GHz, extending the application of the antenna to private 5G (NR band n77).

During this phase, several parametric refinements were made to the slot geometries, the gaps within the CSRRs, and the periodicity of the EBG array. To verify that the meandered paths would provide a return loss (S_{11}) less than −10 dB and a voltage standing wave ratio between 1 and 2 over the target bands of 868 MHz, 2.45 GHz, 4.2 GHz, and 5.8 GHz; current distribution analysis was performed.

The fully labeled design, including the enhanced ground plane and the finalized parameters prior to fabrication, is shown in Figure 3. The detailed geometry and the optimal values for each dimension of the final antenna are presented in Table I, including parameters from the CSRR width to the EBG periodicity, providing a basis for the prototype.

TABLE I. FINAL ANTENNA DESIGN PARAMETERS

Parameter	Value (mm)	Parameter	Value (mm)
Lg	40	Lo	9
Wg	46	Fl	13.5
Lp	31	Fw	3.1
Wp	44	Lw	3.175
Sl	34	Rr	1
Sw	1	Rb	8
Ddg	1.1	Ra	12
Cw	3	Ro	14
Cd	3	Gl	4.5
Fw2	0.6	Gf	7
Lp2	3	Gh	8
Ldg	8	Wdg	45
Ceb	4	Deb	2
Heb	2	Seb	0.20
Geb	1.5	Leb	7

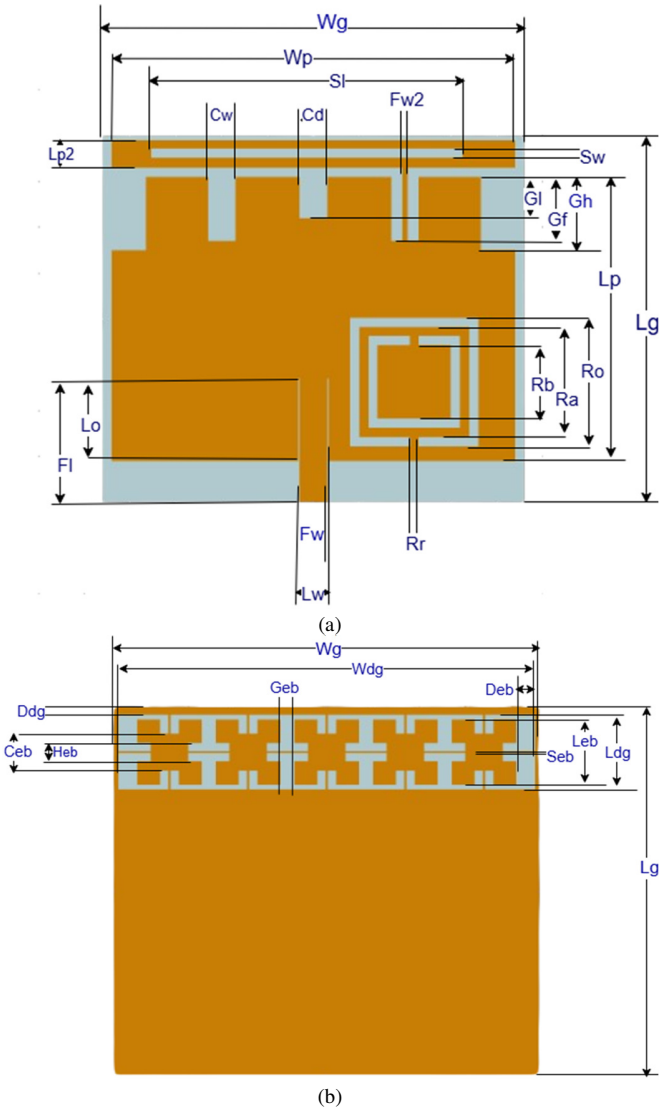

Fig. 3. Structure of the third-stage antenna: (a) top view, (b) bottom view.

III. RESULTS AND DISCUSSION

This section presents a comprehensive analysis of the results obtained from the simulation and experimental validation of the proposed metamaterial-inspired antenna. The evaluation focuses on S-parameters, bandwidth, gain, and a comparative analysis with previously reported works to highlight the effectiveness of the design.

A. Reflection Coefficient (S_{11}) and Bandwidth

The performance of the antenna was first analyzed through simulation using CST Studio Suite, and then measured using a Rohde & Schwarz ZVA50 Vector Network Analyzer (VNA). A comparison between the measured and simulated reflection coefficient is shown in Figure 4. The measurements closely matched the simulations, successfully exciting all the targeted IoT bands.

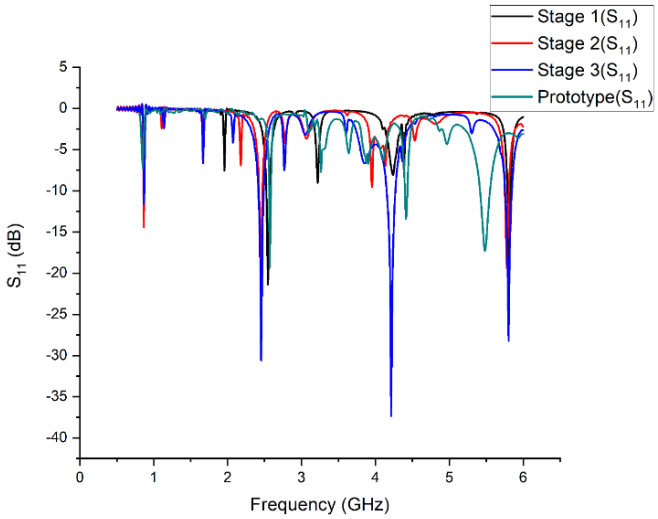

Fig. 4. Simulated and measured return loss (S_{11}) of the antenna during design.

The antenna's bandwidth and resonance characteristics are summarized below:

- 868 MHz band: Measured resonant frequency of 0.8685 GHz with an S_{11} of −11.61 dB. The narrow bandwidth of 7 MHz is expected due to the high Q-factor resulting from the extremely small size achieved through the use of the CSRR and parasitic patch loading. However, this bandwidth is sufficient for standard LPWAN protocols such as LoRa (125–500 kHz channels) and Sigfox (ultra-narrowband ≈ 100 Hz) [19].
- 2.45 GHz band: Deep resonance observed at 2.4525 GHz with an S_{11} of −30.60 dB and a bandwidth of 73 MHz, making this band suitable for Bluetooth, Zigbee, and Wi-Fi based IoT applications.
- 4.2 GHz band: Emergent resonance introduced by the periodic EBG array, peaking at 4.2125 GHz with a return loss of −37.36 dB and a broad bandwidth of 120 MHz.
- 5.8 GHz band: High-frequency resonance at 5.802 GHz with an S_{11} of −28.21 dB and a bandwidth of 90 MHz.

B. Radiation Efficiency

Figure 5 shows the simulated radiation efficiency, illustrating the deliberate trade-off between antenna miniaturization and performance over the operating frequency range. The radiation efficiency at 868 MHz is approximately 5%, which is typical of electrically small antennas with extreme miniaturization techniques (i.e., CSRR loading and parasitic coupling) utilized at sub-GHz frequencies; the result being an extremely high Q-factor of the compact resonator. As a result, a deliberate trade-off between antenna dimensions and radiation efficiency was established. Similar trends in efficiencies have been documented by other researchers who utilize miniaturized metamaterial-inspired antennas at sub-GHz frequencies. However, the overall performance is sufficient for LPWAN applications including LoRa and Sigfox that include link budget designs to allow low power levels while maintaining ultra-compact hardware. Conversely, the antenna has a relatively high radiation efficiency of 80.37% at 2.45 GHz, 79.07% at 4.2 GHz, and 66.21% at 5.8 GHz. These significantly improved radiation efficiency values at the GHz frequencies support the effectiveness of the integrated DGS and uniplanar EBG arrays in reducing losses, improving impedance matching, and reducing surface wave effects.

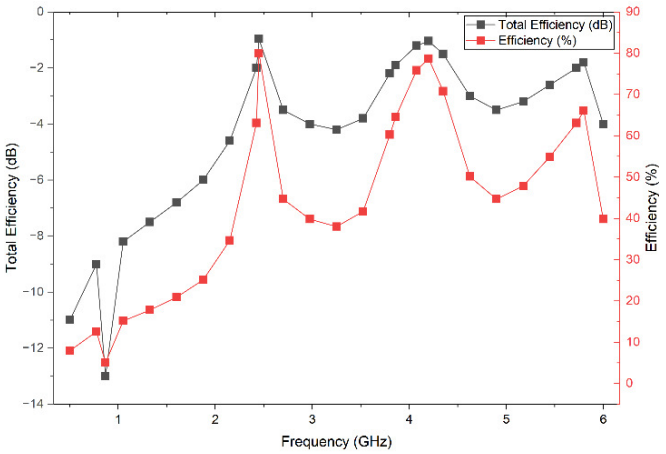

Fig. 5. Radiation efficiency of simulated design.

C. Radiation Patterns

Radiation patterns in both the E-plane and H-plane for the 2D configurations of the antenna are shown in Figure 6. Figure 6 illustrates the antenna's 2D radiation patterns on an angle-by-angle basis as a function of each of the bands in which the antenna operates. The antenna's 2D radiation patterns in the H-plane show a quasi-omnidirectional (all-around) radiation pattern at 868 MHz, which is a critical parameter for IoT node antennas to ensure a stable link margin independent of the node's spatial orientation relative to the access point. Conversely, the E-plane radiation patterns demonstrate a classic dipole-type radiation pattern and are characterized by nulls at 868 MHz. As the operating frequency is increased to the 2.45 GHz, 4.2 GHz, and 5.8 GHz bands, the antenna exhibits a transition from quasi-omnidirectional radiation to a more directional radiation, i.e., broadside radiation. Additionally, the antenna becomes increasingly directive normal to the patch plane as the operating frequency increases. The stability of the 2D radiation patterns for all frequencies, especially the suppression of ripple in the side-lobe level in the E-plane, is due to the presence of the DGS and the uniplanar EBG array, which are used in conjunction to suppress surface wave radiation. The measured 2D radiation patterns indicate that the antenna exhibits a high Front-to-Back (F/B) ratio and a high degree of polarization purity in multi-environmental conditions.

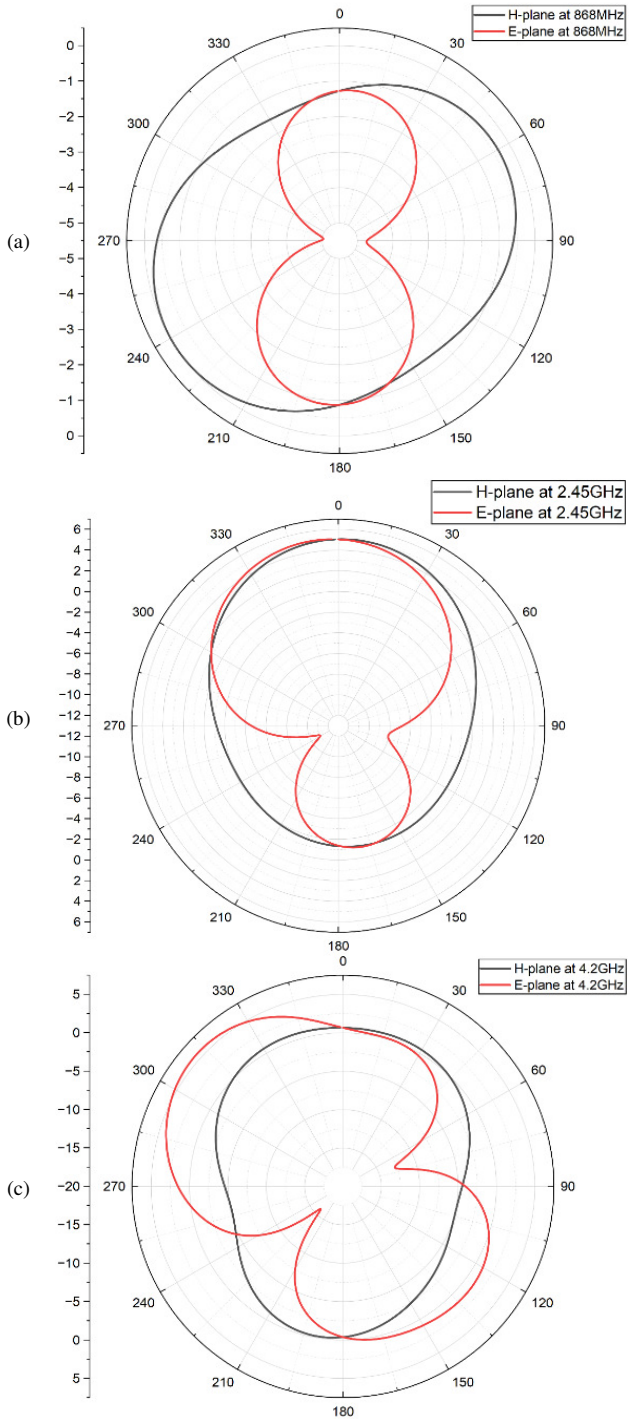

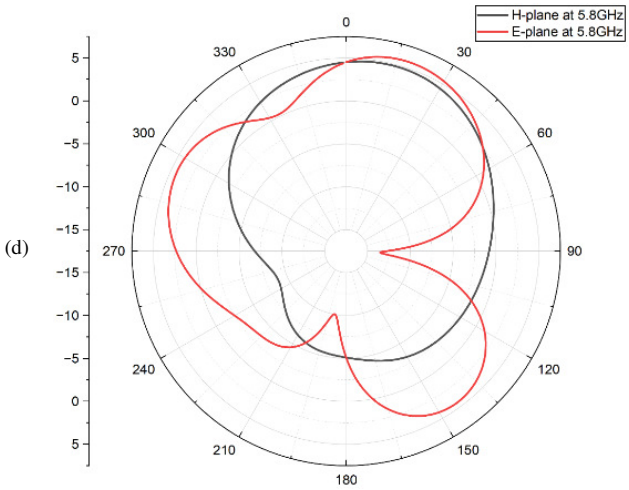

Fig. 6. 2D radiation patterns for both H-plane and E-plane at: (a) 868 MHz, (b) 2.45 GHz, (c) 4.2 GHz, and (d) 5.8 GHz.

D. Far-Field 3D Radiation Characteristics

Figure 7 shows the 3D far-field radiation patterns, which provide an overview of the antenna's power distribution over the entire range of the target frequencies. The 3D radiation pattern of the antenna at the 868 MHz band exhibits a "doughnut" shape, as expected from a quasi-omnidirectional radiator; this behavior supports reliable communication between all types of mobile IoT devices. When increasing the frequency to the 2.45 GHz, 4.2 GHz, and 5.8 GHz bands, a clear trend can be seen toward a broadside directive pattern, where the major portion of the radiated power is concentrated in a single main lobe along the z-axis. The spatial concentration of the radiated power is directly attributed to the uniplanar EBG array and the DGS, as they are effective in reducing surface wave propagation and in minimizing back radiation. Therefore, the 3D results clearly show that the antenna exhibits high radiation efficiency, a stable maximum gain (reaching 4.70 dBi at 4.2 GHz), and suitability for multiple IoT protocols.

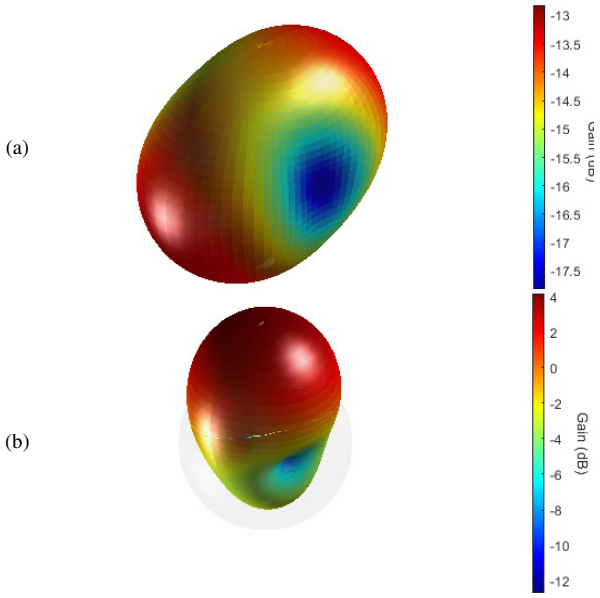

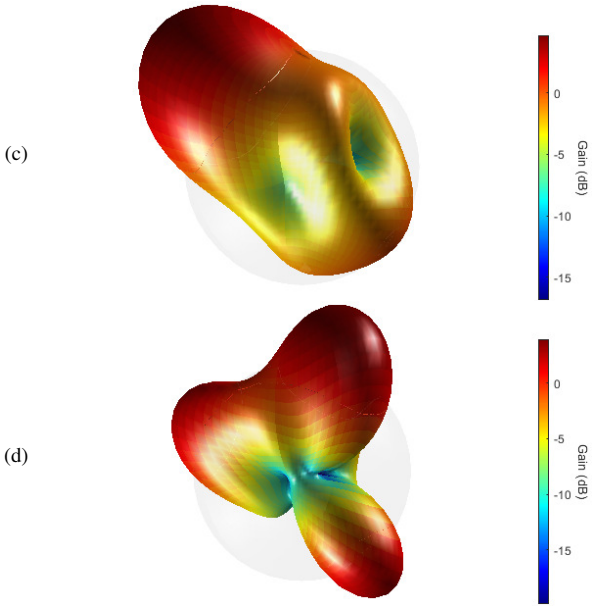

Fig. 7. 3D far-field radiation patterns of the proposed antenna (dBi) at: (a) 868 MHz, (b) 2.45 GHz, (c) 4.2 GHz, and (d) 5.8 GHz.

E. Surface Current Distribution

The surface current distribution shown in Figure 8 illustrates how different regions of the antenna contribute in the generation of the multiple operating bands.

At 868 MHz, the current is distributed around the parasitic patch and the CSRRs, whereas the main patch exhibits minimal current flow, implying that the sub-GHz resonance is primarily produced by the electromagnetic coupling between the CSRRs and the parasitic patch, as well as by the metamaterial loading, which increases the effective electrical length of the structure and enables significant size reduction.

At 2.45 GHz, the current is at the center of the main patch near the feeding port, thus creating a typical TM_{10} mode in a rectangular patch; the CSRRs and parasitic element contribute very little to this mode. At 5.8 GHz, two symmetrical current paths are observed on the main patch, illustrating a higher-order resonant mode that is dominated by the dimensions of the radiator.

At 4.2 GHz, the current distribution is more confined and is influenced by the CSRRs and DGS, confirming that this resonance is a hybrid mode generated by their interaction.

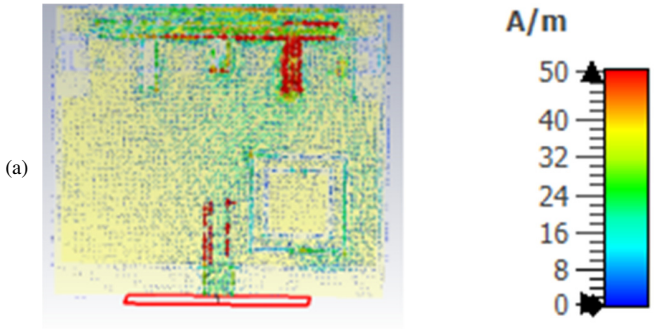

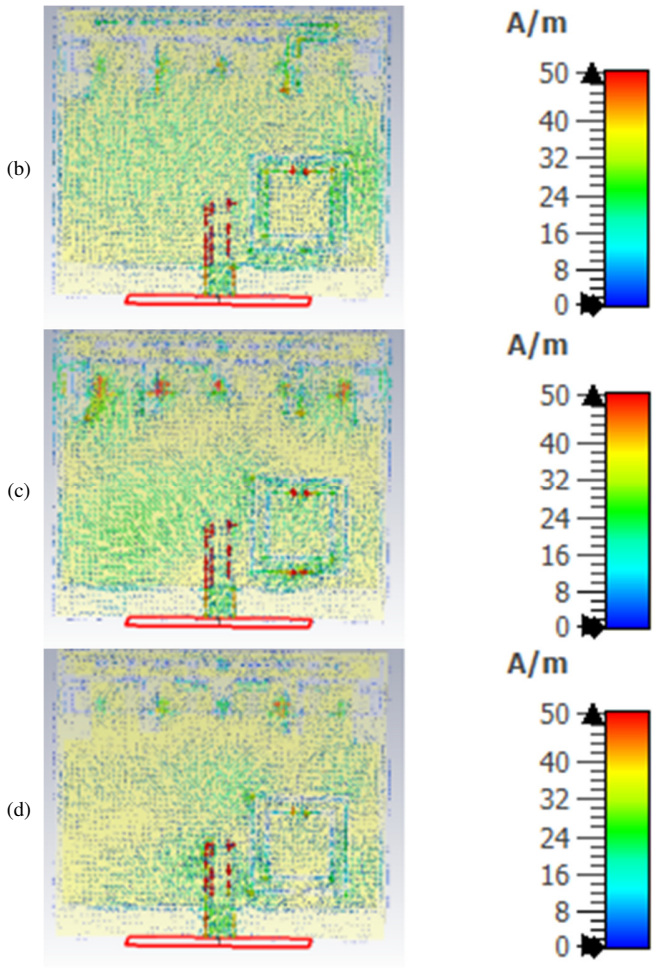

Fig. 8. Surface current distribution of the proposed design at: (a) 868 MHz, (b) 2.45 GHz, (c) 4.2 GHz, and (d) 5.8 GHz.

F. Prototype Fabrication and Measurement Setup

The proposed antenna was fabricated and evaluated using commercially available RF evaluation tools. This section illustrates how the theoretical model was converted to a working hardware prototype. The physical model of the antenna in Figure 9 was created using high-precision ProtoMat S103 milling and Rogers RO4003C material that was 1.524 mm thick. The top view of the antenna in Figure 9(a) shows all components of the radiating patch, the CSRRs that were etched onto the surface, and the electromagnetic coupling between the radiating and parasitic patches. The backside of the antenna in Figure 9(b) shows the DGS and the uniplanar EBG array. The size of the fabricated antenna is quite small (40 mm × 46 mm) but still allows operation over four bands. The test setup in Figure 9(c) shows the antenna attached to a Rohde & Schwarz ZVA50 VNA. The prototype was attached to the VNA through a 50 Ω SMA connector. The VNA was calibrated to provide accurate measurements of the return loss (S_{11}) and bandwidth of the antenna. The results obtained from the prototype measurements showed excellent agreement with those obtained from the CST Studio Suite simulations; however, some minor deviations were observed due to tolerances in manufacturing and the effects of the SMA connector on the antenna's operation. This physical verification confirms the reliability of the designed antenna for use as a component in future IoT and 5G wireless communication systems.

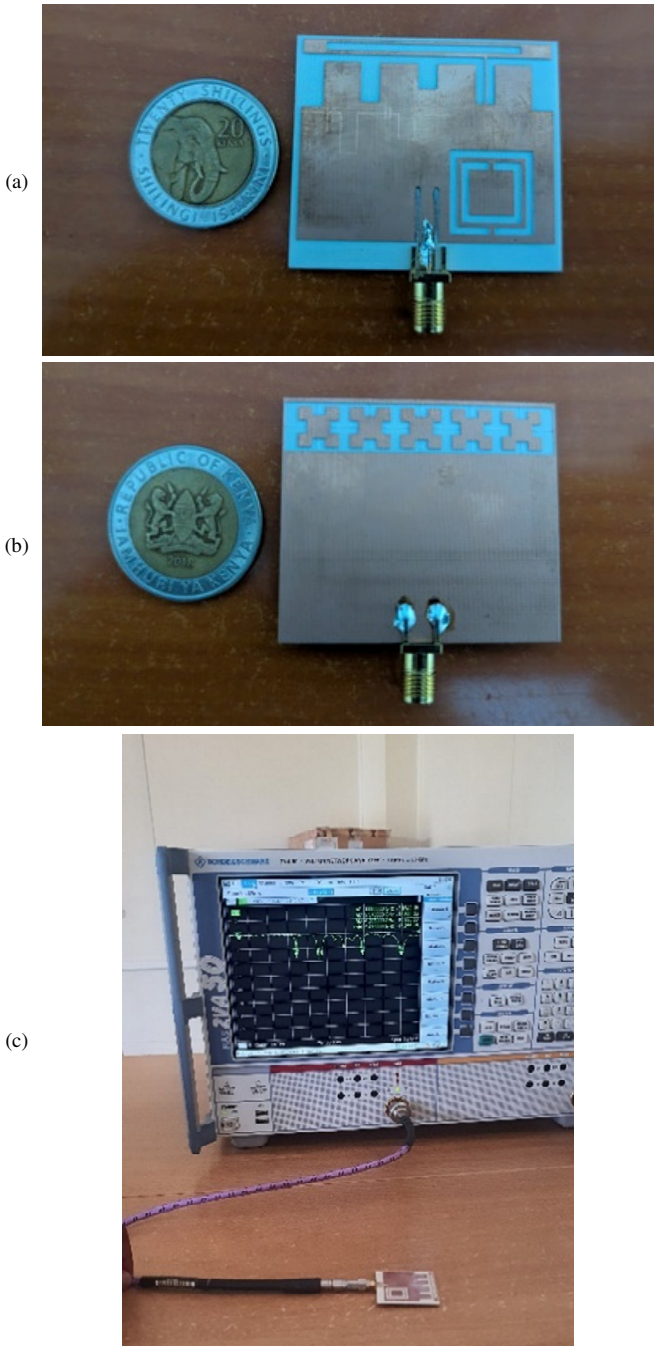

Fig. 9. Prototype of the proposed antenna: (a) fabricated top layer showing CSRRs and parasitic patch, (b) fabricated bottom layer showing DGS and EBG array, (c) experimental measurement setup with the VNA.

To mitigate the issue of integrating a DGS into a practical application, a small air gap or a non-conductive spacer inserted between the defected ground region and the metallic component(s) is advised. This inclusion of a spacer is an

effective integration technique for maintaining the desired current distribution throughout the ground plane while ensuring that the antenna preserves the impedance and radiation properties for which it was designed when integrated with compact IoT hardware.

IV. COMPARISON WITH PREVIOUSLY PUBLISHED WORK

As shown in Table II, although some designs, such as those reported in [4], are able to operate at multiple frequency bands, the proposed antenna achieves a higher maximum gain (4.7 dBi) and additionally includes the 868 MHz band used for LPWAN applications, which are omitted in most other compact designs. The use of metamaterial-inspired CSRRs and EBG structures in this design provides an improved trade-off among bandwidth, physical size, and maximum gain.

TABLE II. COMPARISON WITH PUBLISHED LITERATURE

Ref.	Size (mm)	Operational bands (GHz)	Gain (dBi)	Miniaturization technique
[20]	33 × 22	2.4, 3.7, 5.8	1.43, 0.89, 1	SRR
[21]	40 × 40	2.4, 5.2, 5.8	1.893, 7.17, 6.71	CSRR in DGS configuration
[22]	131.6 × 34	0.915, 2.45, 5.8	1.8, 7, 7	SRR
[23]	86 × 86	0.915, 2.45, 5.8	2, 5.1, 5.7	Multilayer
[4]	45 × 41	0.868, 2.4, 5.8	0.7, 2.3, 3.3	Fractal geometry
[5]	30 × 24.8	2.4, 5.8	−12.38, −4.065	RCSRR
[12]	40 × 60	1.98–3.76, 5.27–10.8	7.85	Textile CVA
[16]	38 × 38	(3.7–4.12), (4.34–4.73), (5.43–6.25), (7.73–8.69), (5.15–5.26)	3.25	Dual ESRRs and EBG
Proposed work	46 × 40	0.868, 2.45, 4.2, 5.8	−12, 4.16, 4.7, 3.94	CSRR, EBG, and DGS

V. CONCLUSION

A compact metamaterial-inspired patch antenna for Internet of Things (IoT) applications was designed, simulated, and fabricated. The proposed antenna operates over four frequency bands at 868 MHz, 2.45 GHz, 4.2 GHz, and 5.8 GHz, achieving multiband functionality within a small footprint of 40 mm × 46 mm. The integration of Complementary Split Ring Resonators (CSRRs) enabled extreme miniaturization at sub-GHz frequencies, the Defected Ground Structure (DGS) improved impedance matching, and the uniplanar Electromagnetic Band Gap (EBG) array suppressed surface waves, resulting in enhanced radiation efficiency and stable gain across all operating bands. Measured results closely matched the simulations, confirming the reliability of the design for practical IoT and private 5G applications. Overall, the proposed antenna offers a compact, low-power solution suitable for IoT applications.

ACKNOWLEDGMENT

The authors would like to express their sincere gratitude to the African Union (AU) for its invaluable support and commitment to advancing scientific research and technological innovation across the continent. This work was supported in part by the African Union Commission, which provided the resources and platform necessary to conduct this research.

REFERENCES

[1] D. G. Arnaoutoglou, T. M. Empliouk, T. N. F. Kaifas, M. T. Chryssomallis, and G. Kyriacou, "A Review of Multifunctional Antenna Designs for Internet of Things," *Electronics*, vol. 13, no. 16, Aug. 2024, Art. no. 3200, https://doi.org/10.3390/electronics13163200.

[2] S. Wang, K. Li, F. Kong, and L. Du, "A miniaturized triple-band planar antenna combing single-cell metamaterial structure and defected ground plane for WLAN/WiMAX applications," *Journal of Electromagnetic Waves and Applications*, vol. 35, no. 3, pp. 357–370, Feb. 2021, https://doi.org/10.1080/09205071.2020.1839569.

[3] A. El Yousfi, A. Lamkaddem, K. A. Abdalmalak, and D. Segovia-Vargas, "A Miniaturized Triple-Band and Dual-Polarized Monopole Antenna Based on a CSRR Perturbed Ground Plane," *IEEE Access*, vol. 9, pp. 164292–164299, 2021, https://doi.org/10.1109/ACCESS.2021.3134497.

[4] E. M. Ceter and G. Poyrazoglu, "Optimization of Fractal Antennas for RFID and Wireless Communication," in *2024 5th International Conference on Communications, Information, Electronic and Energy Systems*, Veliko Tarnovo, Bulgaria, 2024, pp. 1–5, https://doi.org/10.1109/CIEES62939.2024.10811142.

[5] A. Z. Jusoh, N. F. Husain, N. F. A. Malek, F. N. M. Isa, and S. Y. Mohamad, "Design of Miniaturized Antenna for IoT Applications Using Metamaterial," *IIUM Engineering Journal*, vol. 24, no. 1, pp. 122–137, Jan. 2023, https://doi.org/10.31436/iiumej.v24i1.2505.

[6] J. Sam Suresh, G. Soundarya, V. Ganesan, and D. Vedha Vinodha, "Complementary Split Ring Resonator loaded Proximity Coupled Triband Antenna for Sub-6 GHz Use Cases," in *2024 5th International Conference on Smart Electronics and Communication*, Trichy, India, 2024, pp. 121–124, https://doi.org/10.1109/ICOSEC61587.2024.10722126.

[7] T. Jadhav and S. Deshpande, "A Tri-band Planar Inverted-F Antenna with Complementary Split Ring Resonator and Reactive Impedance Surface for Wireless Application," *Engineering, Technology & Applied Science Research*, vol. 12, no. 1, pp. 7988–7992, Feb. 2022, https://doi.org/10.48084/etasr.4592.

[8] D. M. John *et al.*, "A compact flexible four-element dual-band antenna using a unique defective ground decoupling structure for Sub-6 GHz wearable applications," *Results in Engineering*, vol. 21, Mar. 2024, Art. no. 101900, https://doi.org/10.1016/j.rineng.2024.101900.

[9] M. I. Waly *et al.*, "Optimization of a Compact Wearable LoRa Patch Antenna for Vital Sign Monitoring in WBAN Medical Applications Using Machine Learning," *IEEE Access*, vol. 12, pp. 103860–103879, 2024, https://doi.org/10.1109/ACCESS.2024.3434595.

[10] Ruchi, A. Patnaik, and M. V. Kartikeyan, "Compact dual and triple band antennas for 5G-IOT applications," *International Journal of Microwave and Wireless Technologies*, vol. 14, no. 1, pp. 115–122, Feb. 2022, https://doi.org/10.1017/S1759078721000301.

[11] A. A. Megahed, E. H. Abdelhay, M. Abdelazim, and H. Y. M. Soliman, "5G millimeter wave wideband MIMO antenna arrays with high isolation," *EURASIP Journal on Wireless Communications and Networking*, vol. 2023, July 2023, Art. no. 61, https://doi.org/10.1186/s13638-023-02267-y.

[12] N. Nurhayati *et al.*, "A Wearable Coplanar Vivaldi Antenna (CVA) for Internet of Things (IoT)-Based Toddler Stunting Detection," *Engineering, Technology & Applied Science Research*, vol. 15, no. 5, pp. 26564–26575, Oct. 2025, https://doi.org/10.48084/etasr.12430.

[13] N. Nurhayati *et al.*, "Wearable Wideband Textile Coplanar Vivaldi Antenna for Medical and IoT Application," *Progress In Electromagnetics Research C*, vol. 148, pp. 145–156, Oct. 2024, https://doi.org/10.2528/PIERC24080402.

[14] A. J. A. Al-Gburi *et al.*, "Super Compact UWB Monopole Antenna for Small IoT Devices," *Computers, Materials & Continua*, vol. 73, no. 2, pp. 2785–2799, June 2022, https://doi.org/10.32604/cmc.2022.028074.

[15] G. Singla, R. Sharma, R. Khanna, A. Kumar, and A. J. A. Al-Gburi, "Design of a flexible, highly isolated multiband f-meta MIMO antenna for 5G sub-6 GHz applications using the theory of characteristic modes," *Optik*, vol. 345, Feb. 2026, Art. no. 172632, https://doi.org/10.1016/j.ijleo.2025.172632.

[16] S. Arora, S. Sharma, R. Anand, A. Gupta, R. Kumar, and A. J. A. Al-Gburi, "Integration of metamaterials for quintuple band-notched ultra-wideband antennas," *Analog Integrated Circuits and Signal Processing*, vol. 123, no. 1, Feb. 2025, Art. no. 4, https://doi.org/10.1007/s10470-025-02355-7.

[17] P. Jain, P. K. Sahoo, A. D. Khaleel, and A. J. A. Al-Gburi, "Enhanced Prediction of Metamaterial Antenna Parameters Using Advanced Machine Learning Regression Models," *Progress In Electromagnetics Research C*, vol. 146, pp. 1–12, July 2024, https://doi.org/10.2528/PIERC24060901.

[18] H. Pues and A. van de Capelle, "Accurate transmission-line model for the rectangular microstrip antenna," *IEE Proceedings H (Microwaves, Optics and Antennas)*, vol. 131, no. 6, pp. 334–340, Dec. 1984, https://doi.org/10.1049/ip-h-1.1984.0071.

[19] A. Diane, O. Diallo, and E. H. M. Ndoye, "A systematic and comprehensive review on low power wide area network: characteristics, architecture, applications and research challenges," *Discover Internet of Things*, vol. 5, no. 1, Jan. 2025, Art. no. 7, https://doi.org/10.1007/s43926-025-00097-6.

[20] D. H. Abdulzahra, F. Alnahwi, A. S. Abdullah, Y. I. A. Al-Yasir, and R. A. Abd-Alhameed, "A Miniaturized Triple-Band Antenna Based on Square Split Ring for IoT Applications," *Electronics*, vol. 11, no. 18, Sept. 2022, Art. no. 2818, https://doi.org/10.3390/electronics11182818.

[21] R. Roges, P. K. Malik, S. Sharma, S. K. Arora, and F. Maniraguha, "A Miniaturized, Dual-Port, Multiband MIMO with CSRR DGS for Internet of Things Using WLAN Communication Standards," *Wireless Communications and Mobile Computing*, vol. 2023, no. 1, Apr. 2023, Art. no. 3766496, https://doi.org/10.1155/2023/3766496.

[22] M. Abdelkarim, A. Gharsallah, and R. Faouel, "Analysis and Design of a High Gain Multiband Antenna Based on Metamaterials for RFID Applications," *International Journal of RF and Microwave Computer-Aided Engineering*, vol. 2024, no. 1, Mar. 2024, Art. no. 8948916, https://doi.org/10.1155/2024/8948916.

[23] E. Zhang, A. Michel, P. Nepa, and J. Qiu, "Multifeed tri-band circularly polarized antenna for UHF/MW-RFID application," *International Journal of RF and Microwave Computer-Aided Engineering*, vol. 32, no. 1, Oct. 2021, Art. no. e22939, https://doi.org/10.1002/mmce.22939.